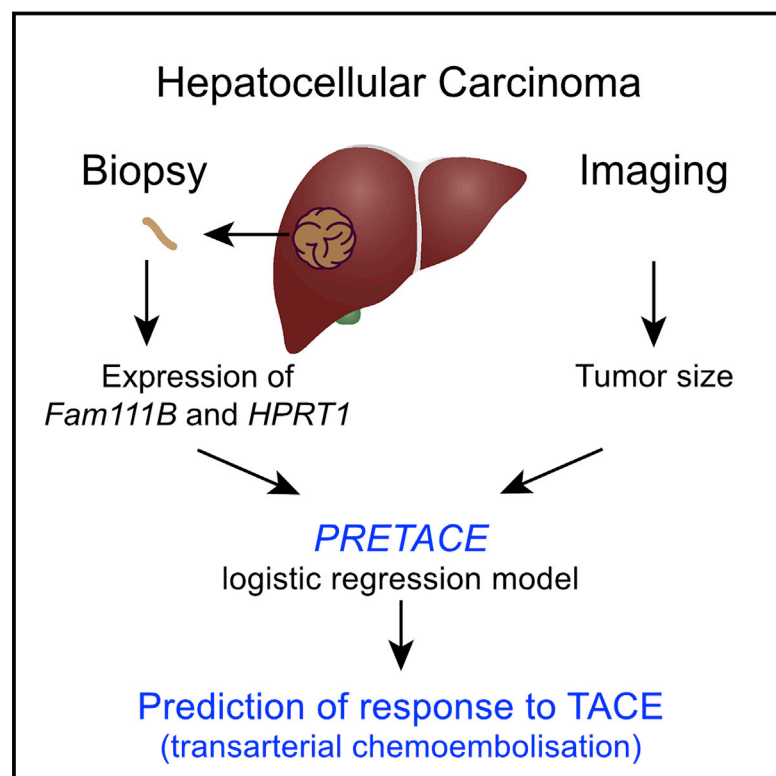


Supervised learning based on tumor imaging and biopsy transcriptomics predicts response of hepatocellular carcinoma to transarterial chemoembolization

Graphical abstract



Authors

Tuyana Boldanova, Geoffrey Fucile, Jan Vosshenrich, ..., Daniel T. Boll, Stefan Wieland, Markus H. Heim

Correspondence

markus.heim@unibas.ch

In brief

Transarterial chemoembolization (TACE) is a widely used first-line therapy for intermediate-stage hepatocellular carcinoma, but not all patients respond to the treatment. Using imaging data and transcriptome data from tumor biopsies, Boldanova et al. develop a logistic regression model that predicts responses to TACE.

Highlights

- Tumor imaging and transcriptomics enables patient selection for good response to TACE
- PRETACE is a LR model based on tumor area and expression of FAM111B and HPRT1
- PRETACE predicts response to TACE with ~90% accuracy



Report

Supervised learning based on tumor imaging and biopsy transcriptomics predicts response of hepatocellular carcinoma to transarterial chemoembolization

Tuyana Boldanova,^{1,2,8} Geoffrey Fucile,^{3,8} Jan Vosshenrich,⁴ Aleksei Suslov,² Caner Ercan,⁵ Mairene Coto-Llerena,⁵ Luigi M. Terracciano,^{5,6,7} Christoph J. Zech,⁴ Daniel T. Boll,⁴ Stefan Wieland,² and Markus H. Heim^{1,2,9,*}

¹Division of Gastroenterology and Hepatology, Clarunis, University Center for Gastrointestinal and Liver Diseases, Basel, Switzerland

²Hepatology, Department of Biomedicine, University Hospital and University of Basel, Basel, Switzerland

³sciCORE Center for Scientific Computing, University of Basel, Basel, Switzerland

⁴Radiology and Nuclear Medicine, University Hospital Basel, Basel, Switzerland

⁵Institute of Medical Genetics and Pathology, University Hospital Basel, Basel, Switzerland

⁶Department of Biomedical Sciences, Humanitas University, Pieve Emanuele, Milan, Italy

⁷IRCCS Humanitas Research Hospital, Rozzano, Milan, Italy

⁸These authors contributed equally

⁹Lead contact

*Correspondence: markus.heim@unibas.ch

<https://doi.org/10.1016/j.xcrm.2021.100444>

SUMMARY

Although transarterial chemoembolization (TACE) is the most widely used treatment for intermediate-stage, unresectable hepatocellular carcinoma (HCC), it is only effective in a subset of patients. In this study, we combine clinical, radiological, and genomics data in supervised machine-learning models toward the development of a clinically applicable predictive classifier of response to TACE in HCC patients. Our study consists of a discovery cohort of 33 tumors through which we identify predictive biomarkers, which are confirmed in a validation cohort. We find that radiological assessment of tumor area and several transcriptomic signatures, primarily the expression of *FAM111B* and *HPRT1*, are most predictive of response to TACE. Logistic regression decision support models consisting of tumor area and RNA-seq gene expression estimates for *FAM111B* and *HPRT1* yield a predictive accuracy of ~90%. Reverse transcription droplet digital PCR (RT-ddPCR) confirms these genes in combination with tumor area as a predictive classifier for response to TACE.

INTRODUCTION

Transarterial chemoembolization (TACE) is the most widely used treatment for intermediate-stage, unresectable hepatocellular carcinoma (HCC).¹ TACE consists of an intra-arterial infusion of a cytotoxic agent followed by embolization of the tumor-feeding blood vessels, resulting in a strong cytotoxic and ischemic effect targeted to the tumor. In conventional TACE, chemotherapeutic drugs such as doxorubicin, epirubicin, cisplatin, or miriplatin are emulsified with Lipiodol. In many centers, TACE is performed with drug-eluting beads (TACE-DEB). The DEB occlude the small tumor-feeding arterioles and obstruct arterial blood flow to the tumor. The chemotherapeutic drug is then released over a 1-week period. The efficacy of TACE was demonstrated in 2 randomized controlled trials,^{2,3} and more recently confirmed in a large systematic review that included data from 10,108 patients.⁴ The objective response rate was 52% and overall survival was 70% at 1 year, 52% at 2 years, and 32% at 5 years, with a median overall survival of 19.4 months.⁴ These numbers indicate that 30% of patients have a poor response to TACE and die within the first year. However, 32% of the patients are alive after 5 years. This suggests that TACE may be very efficacious for a

subgroup of patients. Tumor burden, invasion of the portal vein and its main branches, liver function, and general performance status are criteria to select patients for TACE.⁵ Even in a carefully selected group of patients, however, response to TACE is variable. Moreover, there are alternative treatment options for patients in the intermediate Barcelona Clinic Liver Cancer (BCLC) stage B. Clearly, there is a medical need for predictive biomarkers to guide treatment decisions.

We hypothesized that tumor-intrinsic characteristics are major determinants of the response to TACE. We therefore analyzed pretreatment tumor biopsies using total RNA and whole-exome sequencing, in addition to standard clinical and radiological measures. Our analysis focuses on the prediction of a complete response to treatment at 3 months following TACE. We explored the features that are most informative in predicting the response to TACE in a discovery cohort of 33 tumors, 13 of which showed complete response to TACE at 3 months. Using random forest (RF) models of the discovery cohort, we identified the most informative features and tested ensembles of logistic regression (LR) models against the validation cohort. The most informative gene expression features were tested independently using reverse transcription-digital droplet PCR (RT-ddPCR), which is more



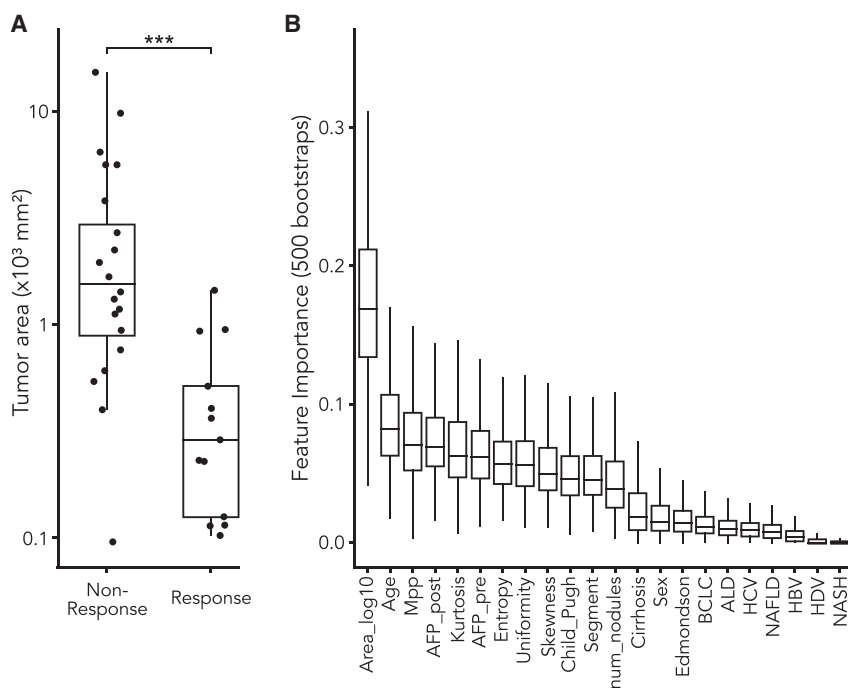


Figure 1. Feature importance in predicting response to TACE

(A) Boxplots showing distribution of tumor area for responder and non-responder tumors (***) $p \leq 0.001$ for Student's t test).

(B) Feature importance scores from a random forest model involving clinical and radiological measurements in prediction of complete response to TACE at 3 months. The boxplots indicate the distribution of scores for 500 bootstraps of training and testing sets using the discovery cohort. Area_log10, log10 of tumor area; Mpp, mean of positive pixels; AFP_pre, pre-treatment α -fetoprotein (AFP) measurement at the time of biopsy; AFP_post, post-treatment AFP measurement 1–3 months after TACE; num_nodules, number of TACEed nodules.

readily accessible in the clinic. We report the distributions of the most informative features for predicting response to TACE in both the discovery and validation cohorts. The biological pathways associated with predictive features are described in the context of carcinogenesis.

RESULTS

Patient clinical data and response to TACE

From May 2008 to July 2017, 30 HCC patients were included in the discovery cohort: 11 (37%) patients with BCLC intermediate-stage HCC and 19 patients (63%) with BCLC early-stage HCC. The early-stage patients were treated with TACE because comorbidities precluded them from surgical treatment, because local ablation therapies were not possible due to the location of the tumor nodules, or because TACE was performed as a bridge-to-transplant treatment. Most of the patients (83%) were male and had cirrhosis of the liver (80%). Alcohol was the main reason for the liver disease (50%), followed by chronic hepatitis C infection (23%). One patient had no liver disease; 77% of the HCCs had Edmondson grade I or II and 23% grade III. The diameter of the tumors ranged from 14 to 155 mm (average 49 mm, median 44 mm). From December 2016 to March 2020, 7 additional patients were included in a validation cohort. The baseline characteristics of the 2 cohorts were consistent (Figure S1C). Patient and tumor characteristics are summarized in Table S1.

In the discovery cohort, radiological complete responses (CRs) were found in 39.4% of biopsied nodules in computed tomography (CT) scans obtained at 3 months after TACE. For the subsequent data analysis, these tumors were classified as “responders,” and all others (including the modified Response Eval-

uation Criteria in Solid Tumors (mRECIST) categories partial response [PR], stable disease [SD], or progressive disease [PD]) as “non-responders.” Treatments, response to TACE, and clinical follow-up of patients in the discovery cohort are shown in Figure S1A. At the time of the last follow-up, 26 of the 30 patients were dead and 4 were alive (3 of them had received transplants). The overall survival in the discovery cohort of patients was 97%, 83%, 63%, and 43% at 6, 12, 18, and 24 months after the baseline imaging. Treatments, response to TACE, and clinical follow-up of patients in the validation cohort are shown in Figure S1B.

Tumor area is predictive of response to TACE

The clinical and radiological information of the study patients at baseline is summarized in Table S1. In a univariate analysis using t test statistics, tumor area was the only feature that was significantly different between responder and non-responder tumors (Figure 1A). In a multivariate analysis, we assessed the importance of these features in predicting response to TACE using RF models. Overall, standard clinical features such as age, sex, etiology of underlying liver disease, tumor stage, and grade, as well as radiological metrics for HCC nodules, were poor predictors of response to TACE treatment, yielding a mean accuracy of 64% across the bootstrap resampling (Figure 1B).

Transcriptomic features are predictive of response to TACE

When considering the whole transcriptome dataset covering 20,126 genes, the first 3 principal components of the normalized count matrix can readily distinguish normal liver, non-tumor, and tumor samples (Figure S2A). There is a hyperplane separating normal liver and non-tumor samples and another that separates tumors from paired non-tumor samples.

We next compared the transcriptome of tumors against their paired non-tumor tissue. There are 341 significantly differentially expressed genes when contrasting tumors versus non-tumors. Using the normalized count matrix of these differentially expressed genes, projection in the first 2 principal components

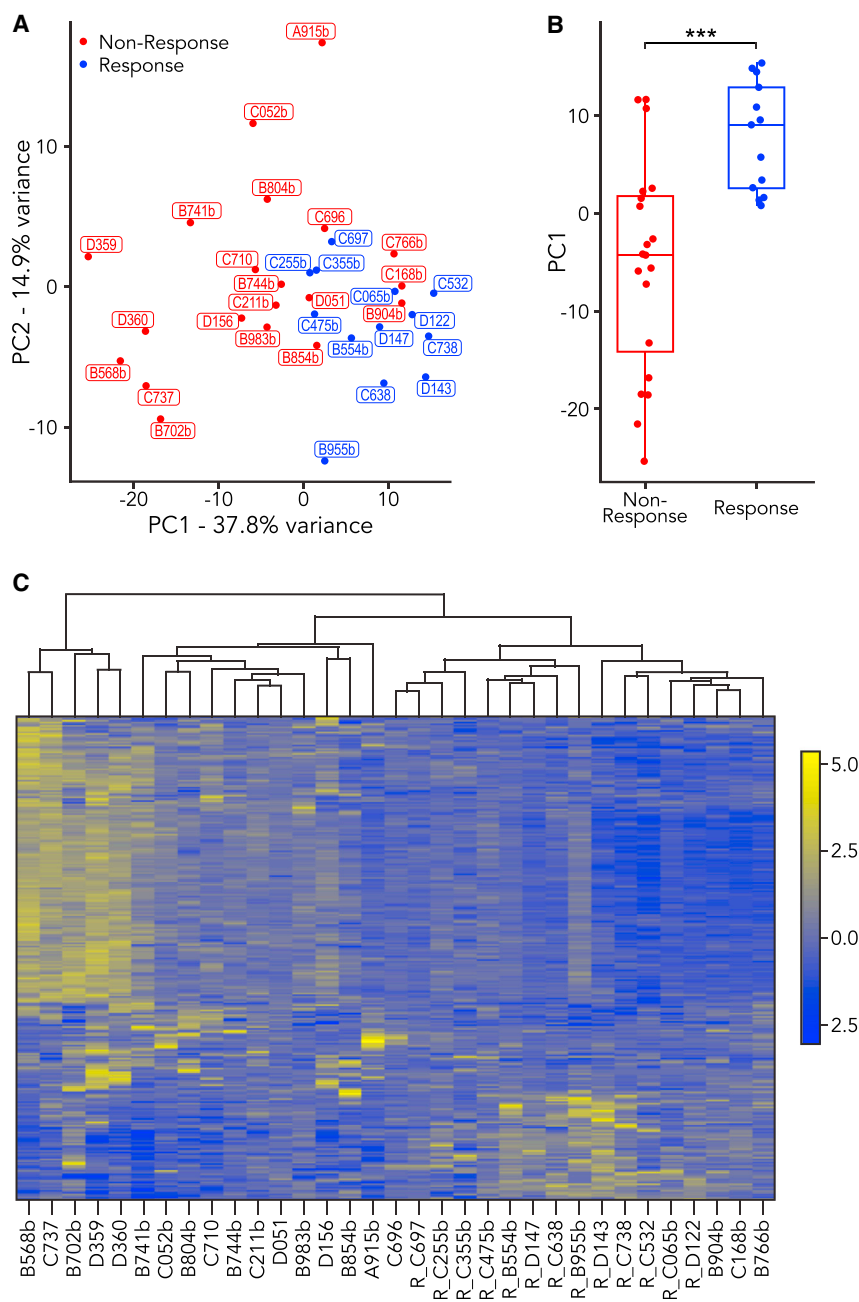


Figure 2. Transcriptomic features are predictive of response to TACE

(A) Scatterplot of the first 2 principal components of the RNA-seq gene expression matrix for significantly differentially expressed genes between responder and non-responder tumors. Expression values were normalized using the variance stabilizing transformation implemented in DESeq2.

(B) Boxplot showing the distribution of projections along the first principal component for responder and non-responder tumors (** $p \leq 0.001$ for Student's t test).

(C) Heatmap showing hierarchically clustered RNA-seq gene expression vectors for differentially expressed genes between responder and non-responder tumors. The responder tumor labels are prefixed with "R_." Expression values were normalized using the variance stabilizing transformation implemented in DESeq2 and scaled before hierarchical clustering using Pearson distance and Ward D2 agglomeration implemented in R version 4.0.3 using the heatmap.2 function from the gplots package.

nificant separation of response and non-response classes along the first principal component (Figure 2B). Hierarchical clustering of this gene expression matrix produces 2 main clusters, which generally split the response and non-response classes (Figure 2C). RF models indicate that FAM111B, hypoxanthine phosphoribosyl-transferase 1 (HPRT1), and the projection along the first principal component are the most informative transcriptomic features in predicting tumor response to TACE (Figure S2D).

Expression of hypoxia and drug efflux pathways are not correlated with response to TACE

Among the genes differentially expressed between responder and non-responder tumors, there is an enrichment of Reactome pathways⁶ related to cell cycle and division, DNA repair, Golgi and endoplasmic reticulum homeostasis, platelet production, and major histocompatibility complex

reveals that the distance between paired non-tumor and tumor samples is significantly greater for non-responder tumors (Figure S2B). Although there is a significant difference in the distribution of these projected distances (Figure S2C), it is not among the most informative features in RF models for response to TACE (Figure S2D).

Considering only tumor samples, differential expression analysis with a contrast of response versus non-response yields 289 significantly differentially expressed genes (Table S2). Decomposition of the matrix of differentially expressed genes by principal-component analysis (PCA) (Figure 2A) indicates a sig-

(MHC) class II presentation (Figure 3). Strikingly absent are several pathways with well-established links to HCC progression, namely the hypoxia-inducible factor 1 α (HIF1 α) hypoxia pathway,^{7,8} the ABC efflux transporter family,^{9,10} and the targets of Notch signaling.^{11,12} We further explored these pathways based on gene sets from previous studies. We used a well-characterized set of HIF1 α target genes that form the core response to hypoxia¹³ (Table S3). Although P-glycoprotein (ABCB1/MDR1) is the canonical transporter for the efflux of chemotherapeutics,¹⁴ we extended our search to the entire set of ABC transporters, which were expressed in our dataset (Table S3). The set

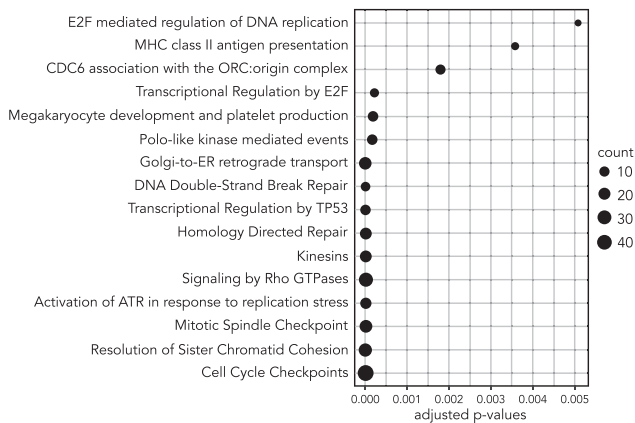


Figure 3. Dotplot showing a subset of the most significantly enriched Reactome pathways among genes differentially expressed between responder and non-responder tumors

p values were adjusted using false discovery rate control. The count indicates the number of genes within the pathway that are differentially expressed.

of Notch target genes was derived from a previous study¹¹ (Table S3). Although none of the 3 pathways are significantly enriched among genes that are differentially expressed between responder and non-responder tumors, subsets of the non-responder tumors have expression values that fall outside the range of expression observed for responder tumors in different genes of these pathways (Figures S3A–S3C). However, we observed a similar pattern for random subsets of expressed genes (Figures S3D–S3F). Although there is no discernible enrichment of differentially expressed Notch target genes, we observed significant differential expression of several genes involved in regulation of Notch signaling, specifically Cdk1, Fos, and HMOX1 (Figures S3G–S3I).

Transcriptomic and radiological features accurately predict response to TACE

RF models clearly indicate that the tumor area at baseline and a small number of transcriptomic features are the most predictive of response to TACE. LR models based on tumor area and the expression of FAM111B and HPRT1 achieve ~90% accuracy in the discovery cohort, with less specificity than sensitivity (Figure 4A). A majority vote ensemble of 500 bootstraps of this LR model using the RNA sequencing (RNA-seq)-derived expression data of FAM111B and HPRT1 and tumor area correctly predicts response to TACE for 7/8 tumors in the validation cohort (data not shown). Apart from response to TACE, there was no significant association between expression levels of these 2 transcripts and baseline characteristics such as BCLC stage or underlying liver disease (data not shown). We next evaluated the performance of similar LR decision support ensembles using semiquantitative measures of FAM111B and HPRT1 at the protein level using immunohistochemical staining of tumor biopsies (Figure S4A). The protein abundances were generally consistent with the cognate RNA-seq gene expression measures; however, the correlation with response to TACE was less significant (Figures S4B and S4C). We then evaluated the expression of FAM111B and HPRT1 using RT-ddPCR, which is generally

more accessible and cost-effective in the clinic than RNA-seq. The RT-ddPCR gene expression estimates were consistent with the RNA-seq data (Figure S4D). LR models based on the RT-ddPCR data achieved only ~80% accuracy in the discovery cohort (Figure 4B); however, bootstrapped ensembles also correctly predicted response to TACE for 7/8 tumors in the validation cohort.

DISCUSSION

Treatment allocation for patients with HCC is currently based largely on radiological staging criteria, liver function, and general performance status.⁵ The widely used BCLC staging system classifies patients into 5 stages and allocates the different treatment modalities according to these stages. However, within a given stage, several treatment options are available, and there is an urgent medical need for additional criteria that guide the allocation of the different treatments within a BCLC staging category. TACE is the first treatment of choice for patients in BCLC stage B (intermediate stage). TACE is highly effective in ~30% of patients,⁴ but for the other 70%, alternative therapies may be a better choice. This question has become even more topical with the increasing number of new systemic combination treatments that are being explored in clinical trials¹⁵ or have even been shown to be effective.¹⁶ In the present study, we investigated whether molecular characteristics extracted from the analysis of treatment-naïve tumor biopsies could predict response to TACE.

Genomic analyses have revealed that the telomerase reverse transcriptase (TERT) promoters CTNNB1 (encoding β -catenin) and TP53 (encoding p53) are frequently mutated in HCC, while genes involved in other critical processes, such as oxidative stress response, chromatin remodeling, and hepatocyte differentiation, are recurrently mutated but in <10% of HCCs.^{17–19} We investigated whether genomic analysis of tumor biopsies could predict the response to TACE. The whole-exome sequencing and variant analysis of our set of pretreatment tumor biopsies yielded a sparse matrix of known cancer mutations (Table S4). Genomic information, however, was not useful for response prediction. Even among the most frequent mutations, there is no discernible distinction between responder and non-responder classes (Table S4).

The transcriptomic data readily distinguish tumor response to TACE, however (Figure 2), confirming our hypothesis that tumor intrinsic characteristics regulate response to treatments. We expected to find an upregulation of pathways known to confer resistance to hypoxia or chemotherapy. However, gene expression patterns of hypoxia, Notch, and drug efflux pathways do not generally distinguish responder and non-responder tumors. It is conceivable that these pathways are predominantly regulated on a post-transcriptional level and could be assessed by proteomic profiling. Intriguingly, several non-responsive tumors fit our expectations: non-responsive tumor D359 has a high expression of 14 HIF1 target genes; tumors C710 and B854b have a high expression of 9 and 8 different ABC transporters, respectively; and B702b and A915b have a high expression of 7 and 6 targets of Notch signaling, respectively. More complex decision tree models may be able to capture these signals for response prediction from larger cohorts. Although the targets of Notch

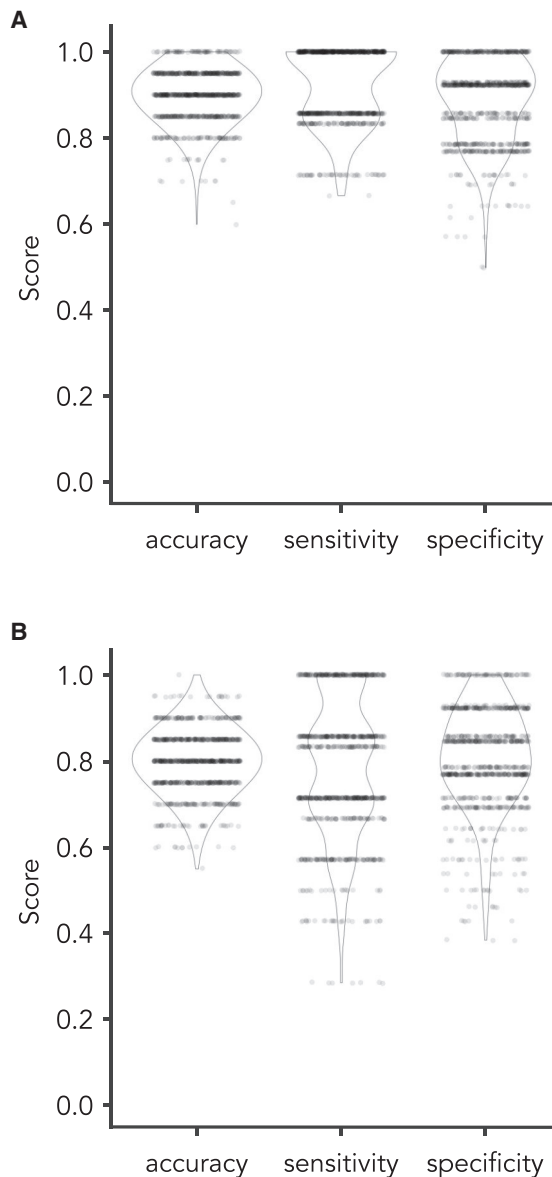


Figure 4. Transcriptomic and radiological features accurately predict response to TACE

(A) Violin plots showing the distribution of accuracy, sensitivity, and specificity scores for logistic regression (LR) models using tumor area at baseline, and RNA-seq gene expression measures of FAM111B and HPRT1. The gene expression measures were normalized using the variance stabilizing transformation implemented in DESeq2, followed by scaling for use in the LR models. The violin plots indicate the distribution of scores for 500 bootstraps of training and testing sets of the discovery cohort.

(B) Violin plots showing the distribution of accuracy, sensitivity, and specificity scores for LR models using tumor area at baseline and RT-ddPCR gene expression measures of FAM111B and HPRT1. The gene expression measures were calculated as the average of 2 technical replicates followed by scaling for use in the LR models. The violin plots indicate the distribution of scores for 500 bootstraps of training and testing sets of the discovery cohort.

signaling are not predictive of response to TACE, several regulators of Notch signaling were significantly differentially expressed between responder and non-responder tumors (Figure S3G–S3I). Cdk1 is directly implicated in Notch signaling via phosphorylation of the Notch intracellular domain,²⁰ Fos is linked to Notch signaling via cross-talk with AP-1,²¹ and HMOX1 is linked to Notch signaling via cross-talk with Nrf2.^{22,23}

Family with sequence similarity 111 member B (FAM111B) encodes a protein with a trypsin-like cysteine/serine peptidase domain. Causative mutations in FAM111B have been identified in patients with congenital poikiloderma.²⁴ The molecular function of FAM111B is not entirely clear. In multiple myeloma, it has been identified as a target gene of TP53,²⁵ and in the human adenocarcinoma cell line A549, FAM111B was shown to degrade the cell-cycle inhibitor p14.²⁶ Furthermore, FAM111B expression was significantly correlated with clinical progression and poor prognosis in lung adenocarcinoma.^{25,26} It is therefore conceivable that in HCC, FAM111B is a surrogate marker for the subclass of TP53 mutant HCCs. In reanalyzing The Cancer Genome Atlas (TCGA) dataset on HCC,¹⁷ we found a significant increase in FAM111B expression in TP53-mutated tumor samples (data not shown).

HPRT plays a central role in the purine salvage pathway and is widely regarded as a housekeeping gene. However, HPRT expression on the mRNA and protein levels is induced by HIF1 α .²⁷ HPRT is most likely a critical pathway that helps preserve the purine nucleotide resources of the cell under hypoxic conditions. One may speculate that HPRT expression is a surrogate marker for tumor cell adaptation to hypoxia, adaptations that protect against the “embolization arm” of TACE.

Given the significant separation of the transcriptomic profile between responder and non-responder tumors, we combined transcriptomic data with clinical data in an LR analysis to identify the most important features that correlate with treatment outcome. Clinicians are well aware of the fact that increasing tumor size reduces the chance of complete response to TACE. Not surprisingly, tumor area was one of the most informative features in our analysis, and tumor area alone in an LR model yields an accuracy of ~75% in predicting response to TACE in the discovery cohort samples. Adding the expression values of just 2 transcripts increased this value to ~90%. The two patients 10 and 13 exemplify the relative contribution and importance of the components of the predict response to TACE (PRETACE) algorithm. In these patients, 2 tumor nodules were treated and showed discrepant responses. In patient 10, the 2 nodules did not differ in size, but in their transcriptome (samples C737 and C738; Figure 2C). However, in patient 13, the 2 nodules have closely related transcriptional profiles (samples C696 and C697; Figure 2C), but C696 is larger than C697. Since RNA-seq from tumor biopsies may not be feasible for the next several years in a routine setting, we explored alternative methods for quantification of HPRT1 and FAM111B. Clinically most useful would be an immunohistochemical staining of histopathological sections. Both proteins can be detected, and their expression can be assessed in a semiquantitative approach (Figures S4A and S4B). However, compared to the quantification of the gene transcripts, immunohistochemistry was less accurate. We next explored the usefulness of RT-ddPCR. LR models using

RT-ddPCR and tumor area (Figure 4B) were overall less accurate in discovery cohort compared to the RNA-seq-based models (Figure 4A) but equally accurate in predicting response to TACE in the validation cohort. Of note, ddPCR has been proven to provide reproducible absolute quantification across different platforms²⁸ and laboratories.²⁹ We therefore propose to implement RT-ddPCR quantification in our PRETACE algorithm.

There are several non-response tumors (B766b, B904b, C168b, and C696) that cluster with response tumors at the level of gene expression (Figure 2C). These non-response tumors do not have extremely large tumor areas; however, one of these patients had extensive comorbidities. We can only speculate why these tumor nodules with a “responder” profile did not respond to TACE, but it could have been due to technical failure of the TACE procedure.

In conclusion, the LR model PRETACE using tumor area and expression values of HPRT1 and FAM111B accurately predicts the response of HCC tumor nodules to TACE. It is a first proof-of-principle that the molecular analysis of HCC tumor biopsies allows us to predict response to treatment. We propose that tumor biopsy-based approaches be explored to identify predictive biomarkers of response to other treatment modalities as well.

Limitations of the study

The study has several limitations. The sample size of the cohorts is small, and we cannot exclude a selection bias. However, our findings are well supported statistically in both the discovery and the validation cohorts. The study is also not powered to analyze the impact of radiological response to TACE at time point 3 months on overall survival. Kaplan-Meier analysis revealed a hazard ratio of 0.60 in favor of TACE responders, but the result was statistically not significant (Figure S1D). Nevertheless, clinical experience strongly suggests that non-response to TACE is associated with poorer prognosis unless patients receive an effective second-line therapy.

STAR★METHODS

Detailed methods are provided in the online version of this paper and include the following:

- **KEY RESOURCES TABLE**
- **RESOURCE AVAILABILITY**
 - Lead contact
 - Materials availability
 - Data and code availability
- **EXPERIMENTAL MODEL AND SUBJECT DETAILS**
- **METHOD DETAILS**
 - CT imaging
 - TACE procedure
 - Radiological response assessment
 - Biopsy procedure
 - Histology/pathology
 - RNA and DNA extraction
 - Next-generation sequencing
 - Reverse-transcription digital droplet PCR (RT-ddPCR)
- **QUANTIFICATION AND STATISTICAL ANALYSIS**
 - Deep sequencing data analysis

- Random forest and logistic regression analysis
- Statistical analysis of baseline characteristics and patient survival

SUPPLEMENTAL INFORMATION

Supplemental information can be found online at <https://doi.org/10.1016/j.xcrm.2021.100444>.

ACKNOWLEDGMENTS

Library preparations and sequencing were performed in the Genomics Facility Basel of the University of Basel and ETH Zurich Department of Biosystems Science and Engineering. Calculations were performed at the sciCORE Scientific Computing Center at the University of Basel. We would like to thank Xueya Wang and Sylvia Ketterer for technical support. The project was funded by the ERC Synergy Grant 609883 (to M.H.H.).

AUTHOR CONTRIBUTIONS

Conceived and designed research project, T.B., G.F., M.C.-L., S.W., and M.H.H. Recruited and followed study patients, T.B. and M.H.H. Obtained biopsies, T.B. and M.H.H. Performed treatments and evaluated response to treatments, J.V., C.J.Z., and D.T.B. Performed the experiments, T.B., A.S., and S.W. Performed histopathological assessment of tissue samples, C.E. and L.M.T. Performed FAM111B and HPRT1 immunohistochemistry and quantification, C.E., M.C.-L., and L.M.T. Performed bioinformatic analysis, G.F. Interpreted the results, T.B., G.F., S.W., and M.H.H. Prepared the figures, S.W., G.F., and T.B. Drafted the manuscript, G.F., J.V., A.S., T.B., S.W., and M.H.H. Revised the manuscript, G.F., S.W., and M.H.H. Obtained the funding, M.H.H. All of the authors approved the final version of the manuscript.

DECLARATION OF INTERESTS

The authors declare no competing interests.

Received: May 27, 2021
Revised: September 3, 2021
Accepted: October 14, 2021
Published: November 16, 2021

REFERENCES

1. Park, J.W., Chen, M., Colombo, M., Roberts, L.R., Schwartz, M., Chen, P.J., Kudo, M., Johnson, P., Wagner, S., Orsini, L.S., and Sherman, M. (2015). Global patterns of hepatocellular carcinoma management from diagnosis to death: the BRIDGE Study. *Liver Int.* *35*, 2155–2166.
2. Llovet, J.M., Real, M.I., Montaña, X., Planas, R., Coll, S., Aponte, J., Ayuso, C., Sala, M., Muchart, J., Solà, R., et al.; Barcelona Liver Cancer Group (2002). Arterial embolisation or chemoembolisation versus symptomatic treatment in patients with unresectable hepatocellular carcinoma: a randomised controlled trial. *Lancet* *359*, 1734–1739.
3. Lo, C.M., Ngan, H., Tso, W.K., Liu, C.L., Lam, C.M., Poon, R.T., Fan, S.T., and Wong, J. (2002). Randomized controlled trial of transarterial lipiodol chemoembolization for unresectable hepatocellular carcinoma. *Hepatology* *35*, 1164–1171.
4. Lencioni, R., de Baere, T., Soulen, M.C., Rilling, W.S., and Geschwind, J.F. (2016). Lipiodol transarterial chemoembolization for hepatocellular carcinoma: a systematic review of efficacy and safety data. *Hepatology* *64*, 106–116.
5. European Association for the Study of the Liver. (2018). EASL Clinical Practice Guidelines: management of hepatocellular carcinoma. *J. Hepatol.* *69*, 182–236.
6. Yu, G., and He, Q.Y. (2016). ReactomePA: an R/Bioconductor package for reactome pathway analysis and visualization. *Mol. Biosyst.* *12*, 477–479.

7. Yang, S.L., Liu, L.P., Jiang, J.X., Xiong, Z.F., He, Q.J., and Wu, C. (2014). The correlation of expression levels of HIF-1 α and HIF-2 α in hepatocellular carcinoma with capsular invasion, portal vein tumor thrombi and patients' clinical outcome. *Jpn. J. Clin. Oncol.* *44*, 159–167.
8. Zheng, S.S., Chen, X.H., Yin, X., and Zhang, B.H. (2013). Prognostic significance of HIF-1 α expression in hepatocellular carcinoma: a meta-analysis. *PLoS ONE* *8*, e65753.
9. Fletcher, J.I., Haber, M., Henderson, M.J., and Norris, M.D. (2010). ABC transporters in cancer: more than just drug efflux pumps. *Nat. Rev. Cancer* *10*, 147–156.
10. Vander Borght, S., Komuta, M., Libbrecht, L., Katoonizadeh, A., Aerts, R., Dymarkowski, S., Verslype, C., Nevens, F., and Roskams, T. (2008). Expression of multidrug resistance-associated protein 1 in hepatocellular carcinoma is associated with a more aggressive tumour phenotype and may reflect a progenitor cell origin. *Liver Int.* *28*, 1370–1380.
11. Villanueva, A., Alsinet, C., Yanger, K., Hoshida, Y., Zong, Y., Toffanin, S., Rodriguez-Carunchio, L., Sole, M., Thung, S., Stanger, B.Z., and Llovet, J.M. (2012). Notch signaling is activated in human hepatocellular carcinoma and induces tumor formation in mice. *Gastroenterology* *143*, 1660–1669.e7.
12. Luiken, S., Fraas, A., Bieg, M., Sugiyanto, R., Goepfert, B., Singer, S., Ploeger, C., Warsow, G., Marquardt, J.U., Sticht, C., et al. (2020). NOTCH target gene HES5 mediates oncogenic and tumor suppressive functions in hepatocarcinogenesis. *Oncogene* *39*, 3128–3144.
13. Benita, Y., Kikuchi, H., Smith, A.D., Zhang, M.Q., Chung, D.C., and Xavier, R.J. (2009). An integrative genomics approach identifies Hypoxia Inducible Factor-1 (HIF-1)-target genes that form the core response to hypoxia. *Nucleic Acids Res.* *37*, 4587–4602.
14. Eckford, P.D., and Sharom, F.J. (2009). ABC efflux pump-based resistance to chemotherapy drugs. *Chem. Rev.* *109*, 2989–3011.
15. Foerster, F., and Galle, P.R. (2021). The Current Landscape of Clinical Trials for Systemic Treatment of HCC. *Cancers (Basel)* *13*, 1962.
16. Finn, R.S., Qin, S., Ikeda, M., Galle, P.R., Ducreux, M., Kim, T.Y., Kudo, M., Breder, V., Merle, P., Kaseb, A.O., et al.; IMbrave150 Investigators (2020). Atezolizumab plus Bevacizumab in Unresectable Hepatocellular Carcinoma. *N. Engl. J. Med.* *382*, 1894–1905.
17. Cancer Genome Atlas Research Network (2017). Comprehensive and Integrative Genomic Characterization of Hepatocellular Carcinoma. *Cell* *169*, 1327–1341.e23.
18. Fujimoto, A., Furuta, M., Totoki, Y., Tsunoda, T., Kato, M., Shiraishi, Y., Tanaka, H., Taniguchi, H., Kawakami, Y., Ueno, M., et al. (2016). Whole-genome mutational landscape and characterization of noncoding and structural mutations in liver cancer. *Nat. Genet.* *48*, 500–509.
19. Fujimoto, A., Totoki, Y., Abe, T., Boroevich, K.A., Hosoda, F., Nguyen, H.H., Aoki, M., Hosono, N., Kubo, M., Miya, F., et al. (2012). Whole-genome sequencing of liver cancers identifies etiological influences on mutation patterns and recurrent mutations in chromatin regulators. *Nat. Genet.* *44*, 760–764.
20. Carrieri, F.A., Murray, P.J., Ditsova, D., Ferris, M.A., Davies, P., and Dale, J.K. (2019). CDK1 and CDK2 regulate NICD1 turnover and the periodicity of the segmentation clock. *EMBO Rep.* *20*, e46436.
21. Nowell, C., and Radtke, F. (2013). Cutaneous Notch signaling in health and disease. *Cold Spring Harb. Perspect. Med.* *3*, a017772.
22. Kim, J.H., Thimmulappa, R.K., Kumar, V., Cui, W., Kumar, S., Kombairaju, P., Zhang, H., Margolick, J., Matsui, W., Macvittie, T., et al. (2014). NRF2-mediated Notch pathway activation enhances hematopoietic reconstitution following myelosuppressive radiation. *J. Clin. Invest.* *124*, 730–741.
23. Sparaneo, A., Fabrizio, F.P., and Muscarella, L.A. (2016). Nrf2 and Notch Signaling in Lung Cancer: Near the Crossroad. *Oxid. Med. Cell. Longev.* *2016*, 7316492.
24. Mercier, S., Küry, S., Shaboodien, G., Houniet, D.T., Khumalo, N.P., Bou-Hanna, C., Bodak, N., Cormier-Daire, V., David, A., Faivre, L., et al. (2013). Mutations in FAM111B cause hereditary fibrosing poikiloderma with tendon contracture, myopathy, and pulmonary fibrosis. *Am. J. Hum. Genet.* *93*, 1100–1107.
25. Sun, H., Liu, K., Huang, J., Sun, Q., Shao, C., Luo, J., Xu, L., Shen, Y., and Ren, B. (2019). FAM111B, a direct target of p53, promotes the malignant process of lung adenocarcinoma. *Oncotargets Ther.* *12*, 2829–2842.
26. Kawasaki, K., Nojima, S., Hijiki, S., Tahara, S., Ohshima, K., Matsui, T., Hori, Y., Kurashige, M., Umeda, D., Kiyokawa, H., et al. (2020). FAM111B enhances proliferation of KRAS-driven lung adenocarcinoma by degrading p16. *Cancer Sci.* *111*, 2635–2646.
27. Wu, J., Bond, C., Chen, P., Chen, M., Li, Y., Shohet, R.V., and Wright, G. (2015). HIF-1 α in the heart: remodeling nucleotide metabolism. *J. Mol. Cell. Cardiol.* *82*, 194–200.
28. Dong, L., Meng, Y., Sui, Z., Wang, J., Wu, L., and Fu, B. (2015). Comparison of four digital PCR platforms for accurate quantification of DNA copy number of a certified plasmid DNA reference material. *Sci. Rep.* *5*, 13174.
29. Pinheiro, L.B., O'Brien, H., Druce, J., Do, H., Kay, P., Daniels, M., You, J., Burke, D., Griffiths, K., and Emslie, K.R. (2017). Interlaboratory Reproducibility of Droplet Digital Polymerase Chain Reaction Using a New DNA Reference Material Format. *Anal. Chem.* *89*, 11243–11251.
30. Dobin, A., Davis, C.A., Schlesinger, F., Drenkow, J., Zaleski, C., Jha, S., Batut, P., Chaisson, M., and Gingeras, T.R. (2013). STAR: ultrafast universal RNA-seq aligner. *Bioinformatics* *29*, 15–21.
31. Bruix, J., Reig, M., and Sherman, M. (2016). Evidence-Based Diagnosis, Staging, and Treatment of Patients With Hepatocellular Carcinoma. *Gastroenterology* *150*, 835–853.
32. Lencioni, R., and Llovet, J.M. (2010). Modified RECIST (mRECIST) assessment for hepatocellular carcinoma. *Semin. Liver Dis.* *30*, 52–60.
33. Nuciforo, S., Fofana, I., Matter, M.S., Blumer, T., Calabrese, D., Boldanova, T., Piscuoglio, S., Wieland, S., Ringnald, F., Schwank, G., et al. (2018). Organoid Models of Human Liver Cancers Derived from Tumor Needle Biopsies. *Cell Rep.* *24*, 1363–1376.
34. Edmondson, H.A., and Steiner, P.E. (1954). Primary carcinoma of the liver: a study of 100 cases among 48,900 necropsies. *Cancer* *7*, 462–503.
35. Liao, Y., Smyth, G.K., and Shi, W. (2014). featureCounts: an efficient general purpose program for assigning sequence reads to genomic features. *Bioinformatics* *30*, 923–930.
36. Love, M.I., Huber, W., and Anders, S. (2014). Moderated estimation of fold change and dispersion for RNA-seq data with DESeq2. *Genome Biol.* *15*, 550.
37. Yu, G., Wang, L.G., Han, Y., and He, Q.Y. (2012). clusterProfiler: an R package for comparing biological themes among gene clusters. *OMICS* *16*, 284–287.

STAR★METHODS

KEY RESOURCES TABLE

REAGENT or RESOURCE	SOURCE	IDENTIFIER
Antibodies		
Polyclonal rabbit anti-human FAM111B Antibody	Invitrogen	Cat#PA5-58474; RRID:AB_2641223
Monoclonal rabbit anti-human HPRT antibody	abcam	Cat#ab109021; RRID:AB_10866312
Biological samples		
Tumor and Non-Tumor liver biopsy tissue	University Hospital Basel	This paper
Critical commercial assays		
ZR-Duet DNA and RNA MiniPrep Plus kit	Zymo Research, Irvine, CA	Cat#D7003
SureSelectXT Clinical Research Exome	Agilent Technologies	Cat#5190-7339
SureSelect Human All Exon V6+COSMIC	Agilent Technologies	Cat#5190-9308
TruSeq Stranded Total RNA Library Prep Kit with Ribo-Zero Gold	Illumina	Cat#20020599
QX200 ddPCR EvaGreen Supermix	Bio-Rad	Cat#1864034
QX200 Droplet Generation Oil for EvaGreen	Bio-Rad	Cat#1864005
DG8 Cartridges for QX200/QX100 Droplet Generator	Bio-Rad	Cat#1864008
DG8 Gaskets for QX200/QX100 Droplet Generator	Bio-Rad	Cat#1863009
PCR Plate Heat Seal, foil, pierceable	Bio-Rad	Cat#1814040
ddPCR 96-Well Plates	Bio-Rad	Cat#12001925
MultiScribe Reverse Transcriptase	Invitrogen	Cat#4311235
Random hexamers	Roche	Cat#11034731001
RNase Inhibitor	Applied Biosystems	Cat# N8080119
10 mM dNTSs	Promega	Cat# U1515
Deposited data		
RNA-sequencing data (41 tumors and 37 adjacent non-tumor tissue and 15 liver biopsies with normal histology)	This paper	European Genome-phenome Archive: EGAS00001005558
Whole-exome sequencing data (122 tumors and 115 adjacent non-tumor liver tissues)	Ng et al., unpublished data	European Genome-phenome Archive: EGAS00001005073
Oligonucleotides		
FAM111B – forward, 5'-CTGGCATAAGA AAGTG TAGCAGCA-3'	This paper	N/A
FAM111B – reverse, 5'-GGGCTGAGTAG ATACTCTCGCTG-3'	This paper	N/A
HPRT1 – forward, 5'-ACATTGTAGCCCT CTGTGTGC-3'	This paper	N/A
HPRT1 – reverse, 5'-AATCCAGCAGGT CAGCAAAGA-3'	This paper	N/A
Software and algorithms		
mint Lesion™ 3.0 software	Mint Medical GmbH, Heidelberg, Germany	https://mint-medical.com
GraphPad Prism 9.2.0	GraphPad Software, San Diego	https://www.graphpad.com
STAR 2.7.1a	Dobin et al., 2013 ³⁰	N/A
R 4.1.0	https://cran.r-project.org/	N/A

(Continued on next page)

Continued		
REAGENT or RESOURCE	SOURCE	IDENTIFIER
DESeq2 1.32.0	https://bioconductor.org/packages/release/bioc/html/DESeq2.html	N/A
scikit-learn 0.24.1	https://scikit-learn.org/	N/A
Other		
PRETACE Python code	This paper	https://github.com/gfucile/PRETACE

RESOURCE AVAILABILITY

Lead contact

Further information and requests for resources and reagents should be directed to and will be fulfilled by the lead contact, Markus H. Heim (markus.heim@unibas.ch).

Materials availability

This study did not generate new unique reagents.

Data and code availability

Data

Sequencing data have been deposited at the European Genome-Phenome Archive and are publicly available as of the date of publication. Accession numbers are listed in the [Key resources table](#).

Code

Software versions and sources and a link to the PRETACE Python code repository are listed in the [Key resources table](#).

EXPERIMENTAL MODEL AND SUBJECT DETAILS

From May 2008 to July 2017, 30 HCC patients undergoing TACE ([Table S1](#)) and 15 control patients with no histopathological liver disease (4 female and 11 male, median age 48 (range 30–62) and 54 (range 33–80), respectively) at the University Hospital Basel were included in our study. The patients undergoing diagnostic tumor and/or liver biopsy at the University Hospital Basel agreed to donate additional biopsies for research purposes. Written informed consent was obtained in accordance with the study protocol approved by the ethics committee of the Northwestern part of Switzerland (authorization number EKNZ 2014-099). The indication for TACE was provided by the institutional multidisciplinary gastrointestinal tumor board. Computed tomography (CT) scans and biopsies of tumors and liver parenchyma were obtained prior to treatment. Tumor staging was done according to the Barcelona Clinic Liver Cancer (BCLC) classification system.³¹

METHOD DETAILS

CT imaging

All patients underwent dynamic CT consisting of four acquisitions: unenhanced, arterial phase (AP), portal venous phase (PVP) and 3-min delayed phase (DP). CT scans were performed using a 128-slice (SOMATOM Definition AS+ or SOMATOM Definition Edge, Siemens Healthineers, Erlangen, Germany) or a 256-slice (SOMATOM Definition Flash, Siemens Healthineers) scanner system. Following the unenhanced scan, 1.2 mL/kg of 370 mg I/ml Iopromide (Ultravist® 370, Bayer Pharma) or 370 mg I/ml Iopamidol (Iopamiro® 370, Bracco S.p.A.) were injected intravenously. Using bolus tracking technique, AP images were acquired 18 s after reaching an enhancement of 100 HU in the descending aorta at the level of the celiac trunk. PVP and DP images were obtained 70 and 180 s after reaching the scan initiation threshold, respectively. CT imaging was done at baseline prior to TACE, and after TACE every 3 months.

Image datasets of all patients and time points were imported into mint Lesion™ 3.0 software (Mint Medical GmbH, Heidelberg, Germany; commercially available) for post-processing. Every lesion was manually segmented on arterial phase images in axial plane (slice thickness 1.5 mm) according to mRECIST 1.1 criteria³² by one radiologist with two years of experience in abdominal imaging (JV). All segmentations were subsequently reviewed by one staff radiologist specialized in abdominal imaging with > 15 years of experience (DTB) and one staff radiologist specialized in abdominal imaging and interventional radiology with > 15 years of experience (CJZ). Disagreements were resolved by consensus. For each tumor nodule, short and long axis were measured (mm) and the largest area was calculated (mm²). CT texture analysis of each segmented ROI was performed automatically by mint Lesion™ software based on gray-level histograms and included the following parameters: entropy, kurtosis, skewness, mean of positive pixels (MPP) and uniformity of positive pixel distribution (UPP).

TACE procedure

TACE procedures were performed or supervised by two interventional radiologists with > 15 and > 10 years of experience. The right femoral artery was punctured using the Seldinger technique and a 4-French Cobra catheter was inserted into the celiac trunk and common hepatic artery, respectively. In case of variant vascular anatomy, also the superior mesenteric artery was catheterized. To visualize feeding arteries of the tumor, digital subtraction angiography was performed and feeding vessels were superselectively intubated with a highly flexible 2.4-French microcatheter. For the following embolization, Doxorubicin-coated 100-300 μm beads were slowly injected under fluoroscopic guidance. The total applied dose per patient was between 100 to 150 mg Doxorubicin. If stasis in the feeding vessel and disappearance of tumor staining was observed earlier, injection was stopped at a lower total Doxorubicin dose, respectively. A closing Dyna-CT was obtained to assess residual staining of treated lesions and vessel blockage.

Radiological response assessment

Response of a biopsied HCC lesion to treatment with TACE as per mRECIST 1.1 criteria was calculated automatically after manual segmentation of the enhancing portions of each lesion on arterial phase images at baseline and all follow-ups. mRECIST 1.1 criteria are: Complete response (CR) = disappearance of any intratumoral arterial enhancement; Partial response (PR) = at least a 30% decrease in the sum of diameters of viable tumor (arterial phase enhancement); Stable disease (SD) = any cases that do not qualify for either partial response or progressive disease; Progressive disease (PD) = an increase of at least 20% in the sum of the diameters of viable (enhancing) tumor. If a lesion did not achieve CR or progressed at the post-therapeutic follow-ups, the institutional multi-disciplinary gastrointestinal tumor conference decided the next therapeutic step.

Biopsy procedure

Biopsies were taken from tumor lesions and from non-tumor liver parenchyma using an US-guided coaxial technique as previously described.³³ In 3 cases we obtained biopsy of the 2 different tumor nodules of the same patient, in 1 patient we obtained 2 biopsies of the same large tumor. 15 normal biopsies from patients (4 female, median age 48 (range 30-62); 11 male, median age 54 (range 33-80) without HCC and with normal liver values were included in the RNaseq analysis as 'normal liver'.

Histology/pathology

Liver biopsies used for routine diagnostic histopathology were processed using standard procedures. Histopathological evaluation was performed by L.M.T., an experienced board-certified pathologist specialized in liver pathology. Tumors were graded according to the Edmondson grading system.³⁴ To be included in the study, tumor biopsies were required to contain > 50% tumor tissue, and non-tumor liver parenchyma samples had to be completely free of cancer cells. Immunohistochemical staining was performed on 4 μm thick sections. Tissue sections were deparaffinized, and subsequently subjected to heat-induced epitope retrieval for 20 minutes in citrate buffer (pH6.0 for HPRT1) and EDTA buffer (pH9.0 for FAM111B). Slides were then stained using anti-FAM111B (Invitrogen PA5-58474; dilution 1:600) and anti-HPRT-1 (Abcam EPR5299; dilution 1:750) on a Leica Bond III IHC staining system (Muntenz, Switzerland) using DAB as chromogen. Images were acquired using an Olympus BX46 microscope (Figure S4A). The expression of tissues was evaluated and scored by two board certified pathologists (L.M.T., C.E.) who were unaware of the clinical data. Each tumor was scored semi quantitatively for each staining by multiplying the proportion of positive cells (%) and the staining intensity score (0, none; 1, weak; 2, moderate; 3, strong).

RNA and DNA extraction

Snap frozen biopsies were crushed in liquid nitrogen, subsequent genomic DNA and total RNA were extracted using the ZR-Duet DNA and RNA MiniPrep Plus kit (Zymo Research) according to the manufacturer's instructions. RNA isolation included a DNase digestion according to the Zymo kit instructions.

Next-generation sequencing

RNA-Seq libraries (TruSeq Stranded Total RNA Ribo-Zero Gold Kit) were sequenced on an Illumina HiSeq 2500 at the Genomics Facility Basel. For whole exome sequencing (WES), whole-exome capture was performed using the SureSelectXT Clinical Research Exome (Agilent Technologies) or SureSelect Human All Exon V6+COSMIC (Agilent Technologies) platforms according to the manufacturer's guidelines. Sequencing was performed on an Illumina HiSeq 2500 at the Genomics Facility Basel according to the manufacturer's guidelines. Paired-end 101-bp reads were generated.

Reverse-transcription digital droplet PCR (RT-ddPCR)

For RT-ddPCR, 250 ng RNA were reverse transcribed using MultiScribe™ Reverse Transcriptase (RT) (Thermo Fischer Scientific) and random hexamer primers (Roche) in a 25 μL reaction volume according to the manufacturer's instructions. Reactions omitting the RT enzyme or the RNA template served as negative controls. 2 μL of RT reaction (or water as negative control) was used for ddPCR in a total volume of 20 μL of 1x QX200 ddPCR EvaGreen Supermix (Bio-Rad, #1864034) and primers (50 nM each). Droplets were generated in the QX200 Droplet Generator (Bio-Rad) with EvaGreen compatible oil (Bio-Rad, #1864006) following the device's instruction manual. Amplification was performed in 96-well plates (Bio-Rad, #12001925) on a C1000 Touch Thermal Cycler (Bio-Rad) using the recommended cycling conditions for EvaGreen Supermix (5 min at 95°C, followed by 40 cycles of 95°C for 30 s

and 60°C for 1 minute, then 1 cycle of 4°C for 5 min and 95°C for 5 min, and a final step of 5 min at 95°C; ramp rate 2°C/sec). After overnight incubation at 4°C, the plate was analyzed in the QX200 Droplet Reader (Bio-Rad), and the absolute copy numbers per 20 ng input RNA for each transcript were calculated with the QuantaSoft (Bio-Rad) software. The following primers were used for FAM111B and HPRT1 specific ddPCR: FAM111B – forward, 5'-CTGGCATAAGAAAGTGTAGCAGCA-3'; reverse, 5'-GGGCTGAGTAGATAC TCTCGCTG-3'; HPRT1 – forward, 5'-ACATTGTAGCCCTCTGTGTGC-3'; reverse, 5'-AATCCAGCAGGTCAGCAAAGA-3'. Primer specificity was confirmed by analyzing the ddPCR products on a 2% agarose gel. Each primer pair produced a single sharp band of the expected size.

QUANTIFICATION AND STATISTICAL ANALYSIS

Deep sequencing data analysis

Sequences were aligned against the NCBI human GRCh38 assembly using STAR³⁰ version 2.7.1a in 2-Pass mode, with an average mapping rate of 85% for uniquely mapped reads corresponding to an average of 47 million aligned reads per sample. Counts were summarized at the gene level using featureCounts from the Subread package using strand information and the NCBI GRCh38 annotations.³⁵ Differential expression was assessed using the DESeq2 Bioconductor package,³⁶ specifically the Wald test for significance of GLM coefficients. We used a significance threshold of 1.5 fold (0.67 log₂-fold) change and adjusted P values < 0.05. Variance stabilizing transformation as implemented in DESeq2 was used as a normalization scheme for principal components analysis and hierarchical clustering. Validation cohort samples were normalized as an ensemble with the discovery cohort for the final models presented in this study. Principal Components Analysis (PCA) was conducted in R using the prcomp function without scaling. Heatmaps were generated using the heatmap.2 function in R, with Pearson distance and Ward D2 agglomeration of row-scaled VST counts.

Pathway enrichment analysis was conducted in R using the ClusterProfiler³⁷ and ReactomePA⁶ packages using hypergeometric tests.

For whole exome sequencing, sequence alignment and single nucleotide variants and indels analysis were performed exactly as described.³³

Random forest and logistic regression analysis

Random Forest (RF) and Logistic Regression (LR) classifiers were developed using the Python scikit-learn library. Selecting subsets of the most informative features was based on an outlier analysis of the distribution of RF model feature importance metrics (Gini impurity index). Training and testing sets were split at 40% and 60% of the discovery dataset, respectively. Given the relatively small number of samples, the accuracy and generalizability of the models were assessed based on bootstrap resampling ($n = 500$). The class labels were balanced for each resampling, such that the difference was less than 15% of the total number of labels in the training set (corresponds to 6 or 7 of each sample class out of 33 tumors in discovery cohort). Exhaustive grid search for parameter optimization indicated that pruning should not be used, and generally the RF models behaved similarly across a wide range of number of trees. Feature vectors were scaled for LR models. The validation set of 8 tumors was evaluated after development of an ensemble classifier obtained from bootstrap resampling of the discovery cohort. A Jupyter Notebook including the Python code used to train the LR models against the discovery cohort and test against the validation cohort has been provided (see [Key resources table](#)). This code (“*PRETACE*” = Predict **RE**sponse to **TACE**) can be used to classify additional samples provided the RNA-Seq expression values are normalized with the discovery cohort samples as per this study using the samples deposited in the EGA (EGAS00001005558).

Statistical analysis of baseline characteristics and patient survival

Fishers's exact tests, chi square tests, Mann-Whitney tests and survival analysis were performed using GraphPad Prism version 9.2.0 for macOS, GraphPad Software, San Diego, California USA, <https://www.graphpad.com>.